IEEE Robotics and Automation Letters (RAL) paper presented at
2024 IEEE/RSJ International Conference on Intelligent Robots and Systems (IROS)
October 14-18, 2024. Abu Dhabi, UAE

Transition Gradient from Standing to Traveling Waves for Energy-Efficient Slope Climbing of a Gecko-Inspired Robot

Worasuchad Haomachai, Zhendong Dai, Poramate Manoonpong*, *Senior Member, IEEE*

***Abstract*—Lateral undulation patterns of a flexible spine, including standing waves, traveling waves, and their transitions, enable agile and versatile locomotion in sprawling animals. Inspired by this, we proposed body-wave transition strategies for energy-efficient inclined-surface climbing of a gecko-inspired robot with a bendable body. Using the robot as a scientific tool, we searched a large space of body movements (i.e., percentage of traveling waves and stride frequency) to explore climbing performance at different slope angles. Consequently, we designed a body-wave strategy to smoothly transition from a standing wave at low speeds to a traveling wave at high speeds to achieve energy-efficient climbing for each slope angle. Through a real robot experiment on the steepest slope (30 degrees), we demonstrated that the robot can reduce energy consumption by 7% compared to climbing with a constant-body movement owing to the transition gradient from standing to traveling waves with an optimal speed. To this end, our study can pave the way for the development of climbing robots that utilize multiple body movement patterns with smooth transitions. Moreover, it can make a valuable contribution to biologists by formulating a novel hypothesis concerning the energy efficiency of gecko climbing.**

***Index Terms*—Climbing robot, gecko-inspired robot, lateral undulation pattern, traveling waves, body wave transition**

I. Introduction

LATERAL undulation of the flexible spine makes sprawling animals capable of robustly negotiation challenging natural environment with efficiency and grace. The intercoordination between the flexible spine and limbs of sprawling animals, such as geckos, lizards, and salamanders, results in versatile locomotor behaviors, including walking, swimming, and climbing. Specifically, they not only perform various locomotion modes but also employ distinct lateral undulation patterns in specific behaviors and smoothly transition between different body patterns depending on their speed. Body patterns, including standing waves, traveling waves, and their transitions, play a crucial role in obtaining agile and versatile locomotor capabilities. In particular, geckos exhibit different lateral undulation patterns during slow-speed trotting and high-speed running, with standing and traveling waves, respectively [1]. These capabilities have attracted the interest of researchers who intend to develop robots with lateral body movements to mimic animal locomotor skills.

W. Haomachai, Z. Dai and P. Manoonpong are with the Institute of Bio-inspired Structure and Surface Engineering, College of Mechanical and Electrical Engineering, Nanjing University of Aeronautics and Astronautics, Nanjing, China. P. Manoonpong is also with Bio-inspired Robotics & Neural Engineering Lab, School of Information Science & Technology, Vidyasirimedhi Institute of Science & Technology, Rayong, Thailand. *Corresponding author: poma@nuaa.edu.cn, poramate.m@vistec.ac.th

Previous studies on sprawling posture robots have focused on two developmental streamlines. The first streamline focuses on developing sprawling robots capable of terrestrial walking, aquatic stepping, and/or swimming. They were mostly designed with an elongated body morphology comprising bendable segments that enable lateral undulation capabilities to improve locomotion. For instance, amphibious robots with 8-11 degrees of freedom (DoFs) of a bendable segmented spine, such as salamander-inspired robots [2] [3], can achieve multimodal locomotion modes and transition from walking to swimming and vice versa. This was primarily achieved owing to the utilization of both undulation patterns, i.e., standing and traveling waves for walking and swimming, respectively. A lizard robot coordinates its tiny limbs and long body to exhibit a traveling wave and consequently improve sand-swimming performance [4]. Moreover, salamander-like robots can achieve path following on flat terrain via lateral undulation [5]. A study by [5] also demonstrated that exhibiting a traveling wave helped improve the balance of the robot during turning. Although sprawling posture robots with elongated bodies have achieved impressive results in locomotion skills, such as walking, turning, and swimming, none of them have performed a detailed investigation of body patterns with respect to locomotion speed and smooth transition mechanisms that are thought to play a crucial role in locomotion performance, as found in salamanders [6]. Particularly, locomotion capabilities involving a transition gradient from a standing wave to a traveling wave have not yet been fully studied in robotics.

In addition to the first streamline, the development of sprawling robots focuses on climbing capabilities. For example, gecko-inspired robots primarily emphasize special foot structures to enable the use of adhesive materials with peeling mechanism for climbing smooth inclined slopes [7] [8], walls [9], ceilings [10] and uneven pipes [11]. While such robots can exhibit climbing abilities, they lack the utilization of multiple body undulation patterns for efficient climbing, as found in their animal counterparts. This is because they were designed with a rigid body [7]-[11] or some had segmented bodies driven by two actuators, which is the minimum DoF required to enable a traveling wave. However, they only undulated with a single standing-wave pattern [12]. Unfortunately, in the field of biology, no experimental data have been collected on geckos regarding the transition gradient from a standing wave to a traveling wave during climbing. This raises the research question: "What is the efficient strategy of transition from standing wave at low locomotion speed to traveling wave at

high locomotion speed for climbing?"

To address this question, we used our gecko-inspired robot (called Slalom) [13] with 3-DoFs bendable body designed based on a gecko structure to explore the large space of lateral undulation patterns from standing to traveling waves with different locomotion speeds for inclined surface climbing. Investigating the gradient of body patterns between purely standing (C-shaped) and extremely traveling waves (S-shaped) enabled us to analyze robot climbing performance (i.e., cost of transport (CoT) and locomotion speed) and design an energy-efficient strategy of simultaneous body-wave transitions for climbing enhancement.

The contributions of this study are summarized as follows: i) to efficiently explore climbing performance, we present a systematic method using the response surface method (RSM) to investigate the large space of body movement parameters (i.e., percentage of traveling waves (%Trav) and stride frequency) when the robot climbs at different slope angles, ii) we propose body-wave transition strategies to exhibit a continuum of motions by altering body wave patterns with optimal speeds to obtain energy-efficient climbing for each slope angle, iii) we perform physical robot climbing with camera tracking analysis at a 30-degree slope angle and compare climbing performance with and without body-wave transition strategies, iv) to the best of our knowledge, this study is the first to investigate the transition gradient of the lateral undulation of a gecko-inspired robot for climbing enhancement. This may contribute to the development of a novel hypothesis regarding gecko climbing in relation to energy efficiency while offering a framework for identifying the essential data required from animals to discover fundamental knowledge.

II. Gecko-inspired lateral undulation pattern

In our previous studies involving the lateral undulation patterns of the flexible bodies of geckos [1] [14], we observed that geckos exhibited an increase in stride frequency to enhance their locomotion velocity. At low speeds, their body movement exhibited a waveform characterized by single-peak curves in a standing wave. Conversely, at high speeds, the waveform of their body movement propagated from the head to the tail in a traveling wave.

In the standing wave, the flexible spine almost formed a C-shape. Throughout a stride cycle, the trunk exhibited a fixed maximum lateral flexion, in which all points on the trunk reached their maximum displacement simultaneously [15]. At least one point has zero lateral velocity and is described as a "node" that does not oscillate laterally [16]. The nodes are mostly situated in proximity to the pectoral or pelvic girdle, where the spine primarily rotates along the dorsoventral axis. The absence of nodes is a defining characteristic of traveling waves.

In a traveling wave, every point along the body oscillates laterally in the transverse plane. The oscillations propagate sequentially along the longitudinal axis of the body from the head to the tail, while the points of greatest excursion and minimum flexion do not remain stationary. A standing wave can be considered a particular instance of a traveling wave. Experimental data collected from biological observations indicated that geckos exhibit certain waveform peculiarities in standing and traveling waves. However, experimental data regarding the transition from standing to traveling waves are lacking. Therefore, we extended our knowledge from the biological to robotics domains by investigating the transition gradient of body patterns between standing and traveling waves for energy-efficient climbing (see below).

A. Lateral Undulation Pattern of Geckos

We began with a quantitative analysis of the flexible body movement of the Gekko gecko based on experimental videos recorded using a high-speed camera. Using a cartesian coordinate representation, ten tracking markers that were placed on the bodies of geckos were converted into a continuous curve that represented the body's midline (see Fig. 1A). Consequently, three joints[1] with equal distances between them were augmented over the midline to reproduce the curvature of the gecko's body during locomotion. Therefore, we demonstrated the joint trajectories of a gecko's body with three degrees of freedom, which is the optimal number for a robot's body (see Fig. 1B) [13]. The animal experiments were conducted in accordance with the Guidelines for Laboratory Animal Management in China and the approval of the Jiangsu Association for Laboratory Animal Science (Jiangsu, China, approved file no 2019-152).

The data processing of the axial movements of the geckos enabled us to investigate the phase relationships of each joint. Figure 1 illustrates an example of a traveling wave during stride locomotion. The time evolutions of the body posture and joint trajectories are shown in Fig. 1A and Fig. 1B, respectively. Consequently, the joint trajectories of a full-cycle stride period (P) were transformed into the same alignment, allowing the measurement of their phase relationship (see Fig. 1C). Finally, we observed that the phase difference between body joints 1 (b1) and 2 (b2) was approximately four times greater than that of the phase difference between body joints 2 (b2) and 3 (b3). More precisely, phase of b2 was shifted from b1 around $\frac{\pi}{3}$ radians and phase of b3 was shifted from b2 around $\frac{\pi}{12}$ radians. Hence, the phase relationship ratio of the body joint was defined as ψ**:**0.25ψ. This ratio indicates that the phase of b2 shifts from b1 by ψ, whereas that of b3 shifts from b2 by 0.25ψ.

Moreover, as reported previously, a standing wave is a special case of a traveling wave. Specifically, all the body joints have the same phase for a standing wave or $\psi = 0$ in the phase relationship ratio. This indicates that the above analysis of the traveling wave is also applicable to the case of a standing wave. In this study, we used the observed gecko phase relationship ratio to generate different waveforms while maintaining a consistent phase ratio.

B. Waveform Representation

To arrive at a control body pattern for a gecko-inspired robot, a mathematical understanding of waveform measurement and representation is a critical step. We used the wave-

[1]Three joints is an optimal number to replicate the gecko's body flexion.

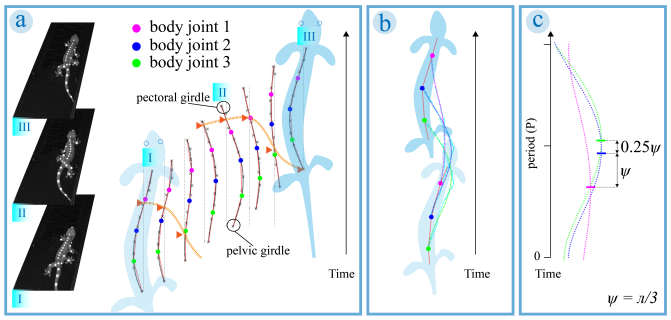

Fig. 1: Quantitative analysis of a flexible body movement of the Gekko gecko. (A) body posture of a gecko with three key indicated joints during locomotion. This body movement exhibits a traveling wave such that the point (orange triangle) of minimum lateral displacement propagates consecutively along the body. (B) trajectory of the three body joints. (C) the joint trajectories are transformed into the same alignment to compare their phases. The pink, blue, and green short vertical lines represent the peaks of joint trajectories 1, 2, and 3, respectively, allowing us to measure the phase difference between them.

form index $W = D_{std} - D_{trv}, D_x = \min_{\Theta\in[0,2\pi]}|\mathbf{r} - e^{i\Theta}\mathbf{r_x}|$, which was based on the body-pattern evaluation method [17].

$$\mathbf{r} = \{e^{i\Phi_{b1}}, e^{i\Phi_{b2}}, e^{i\Phi_{b3}}\}, \quad \Phi_j = \phi_j - \phi_{ref}, \tag{1}$$

$$\mathbf{r_{std}} = \{1, 1, 1\}, \quad \mathbf{r_{trv}} = \{1, e^{-i\frac{2\pi}{3}}, e^{-i\frac{5\pi}{6}}\}, \tag{2}$$

where D_{std} and D_{trv} denote the distances of standing and traveling waves, respectively. $\mathbf{r}$, $\mathbf{r_{std}}$, and $\mathbf{r_{trv}}$ denote the phase relationships between the body joint angles ($j \in$ {b1, b2, b3}) of the exhibited wave, standing wave, and traveling wave, respectively. Φ_j is the phase relationship between the phases of joint j (ϕ_j) and reference joint (ϕ_{ref}), in which body joint 1 (b1) was defined as our reference joint, i.e., $\phi_{ref} \equiv \phi_{b1}$. The distance serves as a metric to evaluate body wave characteristics, indicating that the emergence of a standing wave results in a lower value of D_{std} and a higher value of D_{trv}. By contrast, the emergence of a traveling wave results in a higher value of D_{std} and a lower value of D_{trv}. Hence, the emergence of positive values of the waveform index W corresponds to the occurrence of traveling waves, whereas the negative values of W indicate the emergence of standing waves. When W is equal to zero, it signifies the emergence of intermediate waves. For additional information on the derivation method, please refer to [17].

In this study, we mapped the negative/positive constant number of the waveform index to the percentage of traveling waves (%Trav) for interpretation, such that the standing wave is represented as 0 %Trav, in which all body joints have the same phase (i.e., the phase relationship of body joints $\mathbf{r_{std}}$ is shown in Equation 2). The greatest difference in body phase, as described by Equation 2 with $\mathbf{r_{trv}}$, indicates the highest proportion of traveling waves, which is represented by 100 %Trav. Thus, we can map the traveling wave of gecko's body in Fig. 1C, which exhibits a phase-relationship ratio of ψ=$\frac{\pi}{3}$ and W = 0 to 50 %Trav. Note that %Trav is used to represent the body pattern throughout this study.

III. Slalom, a Gecko-inspired Robot

A. Robot Simulation and Hardware Setup

A gecko-inspired robot, Slalom, was used in this study. Its structure is composed of four identical legs, each consisting of four joints. Joints 1-3 are associated with the shoulder and hip joints of the front and hind legs, respectively. Joint 1 ($j1$) facilitates motion in both forward and backward directions, joint 2 ($j2$) allows for elevation and depression of the leg, and joint 3 ($j3$) provides the attachment and detachment of the foot. Joint 4 ($j4$) is associated with the elbow and knee joints of the front and hind legs, respectively. This joint facilitates foot extension and flexion. The passive ball joint allows the foot to adapt to the ground. Slalom has 19 active joints, with four located on each leg and three on the body, which is the optimal number of joints for a body. Its overall weight is 2.45 kg.

We simulated a gecko-inspired robot using the physical simulation software, CoppeliaSim, with the Vortex physics engine developed by CM Labs. For the physical robot, the mechanical structure was constructed using 3D printing with nylon material. Neural control (described below) was developed based on a robot operating system for driving the actuators [13].

B. Central Pattern Generator (CPG)-based Neural Control

Slalom uses CPG-based neural control (Fig. 2A) to generate a basic gecko-like trot gait. The control consists of three main layers: i) a CPG mechanism with neuromodulation (MI) to generate different rhythmic patterns and shunting inhibition (SI) to alter body joint movements, ii) neural CPG post-processing (PCPG) was used to shape the CPG output signals and consequently obtain the desired leg joint movements, and the delay line unit (τ) was used to obtain different body waveforms, and iii) motor neurons to send final motor position commands to all the joints of the robot.

The CPG mechanism was based on our previous study [13], which used a recurrent neural network with two fully connected neurons to generate a rhythmic signal for locomotion. The weights between both recurrent neurons were determined as $W_{12} = 0.18 + MI, W_{21} = -W_{12}$, and $W_{11,22} = 1.4$. MI is an extrinsic modulatory input for generating different stride frequencies of the trot gait. In this study, MI was set to 0.12, 0.18, 0.24, and 0.30 resulting in stride frequencies of 0.16 Hz, 0.33 Hz, 0.47 Hz, and 0.58 Hz, respectively. The maximum stride frequency was limited to 0.58 Hz because the real robot hardware is unable to follow the high driving frequency properly.

The output of CPG neuron 1 (c_1) was passed to the motor neurons through both shunting inhibition with delay line units and CPG postprocessing for driving the body and leg movements, respectively (Fig. 2A). For the body movements, we manually controlled the inhibitory input by setting it to either inactive ($I = 0$) or active ($I = 1$). By setting $I = 0$, the robot

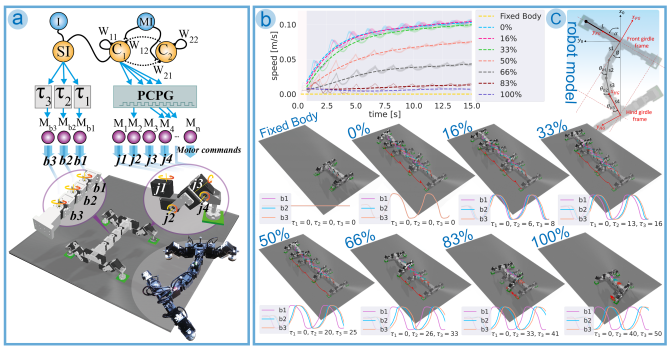

Fig. 2: (A) System overview of the CPG-based neural controller and gecko-inspired robot. The neural circuit drives the body and leg separately through their motor neurons. The purple circle provided a detailed description of the location of each motor neuron on the robot and the direction of the joint movement. The simulated robot's posture shows the default motor position of the body and legs, whereas the right side illustrates the physical robot bending its body with its default leg position. (B) Velocity profile and robot postures with the signals controlling the body joints (b1, b2, b3) when moving at different body patterns from fixed-body to standing wave (0 %Trav) and varying percentages of traveling waves (16 to 100 %Trav). All of them have a stride frequency of 0.33 Hz. (C) Additional analysis of locomotion performance based on a geometrical model of the robot can be accessed at https://bit.ly/3PdOUpI.

undulates its bendable body while locomoting; otherwise, the body is fixed (i.e., $I = 1$, fixed body shown in Fig. 2B). Consequently, delay line units ($\tau_{1,2,3}$) were used to shift the phase of the original c_1 to obtain three different phase signals for driving each body joint separately, aiming to achieve body wave patterns. Additional information on the delay line mechanism can be accessed at https://bit.ly/3PdOUpI.

Regarding leg movement, the CPG postprocessing (PCPG) units also received the c_1 signal to shape it into simple stepping-like signals. The outputs of the PCPG unit were transmitted directly to the motor neurons to control the legs. It is important to note that we only controlled leg joint 2 ($j2$) of each leg to enable the elevation and depression of the leg, By contrast, leg joints 1, 3, and 4 were fixed at a constant default position (see Fig. 2A) to perform a simple leg trajectory that can meet the bare minimum for controlling a robot with body undulations. To achieve a trot gait characterized by the synchronous occurrence of the swing and stance phases in the diagonal legs, providing identical signals to the diagonal joints is necessary, while the remaining diagonal joints receive inverted signals (180° phase-shifted).

Figure 2B depicts an example of the velocity profiles and robot postures with the signals controlling the body joints (b1, b2, b3) when the robot moves on a 0-degree slope angle with various percentages of traveling waves (%Trav). All of them move at a stride frequency of 0.33 Hz. The fixed-body robot was unable to move forward because leg joint 2 was controlled only to move up and down, whereas forward and backward motions were produced by body undulation. Therefore, the fixed-body robot could not propel itself without body undulations. The standing waves (0 %Trav), 16 %Trav, and 33 %Trav seemed to perform at a higher speed; however, the speed decreased after 50 %Trav and got struck at 100 %Trav. This suggests that altering body patterns results in various motion behaviors that influence the locomotion capabilities of the robot. Further discussion on this matter is presented in the Discussion and Conclusion sections.

IV. Experimental Setup and Results

We proposed a systematic analysis to efficiently explore a large space of body movements by using SMR in simulations and real environments. The simulation experiments were conducted at different stride frequencies of 0.16, 0.33, 0.47, and 0.58 Hz to study the robot climbing performance (i.e., cost of transport (CoT) and speed) when climbing with different body patterns (0, 16, 33, 50, 66, 83, and 100 %Trav). Different slope angles (0, 15, 20, 25, and 30 degrees) were also used for the simulation. The CoT and speed ware captured while the robot moved at 1st, 2nd, and 3rd stride[2] for 10 trials. Based on our previous work [13], which was set up with a simple leg trajectory and without adhesive foot material, the steepest slope the robot can climb is 30 degrees.

The calculation of CoT was performed using CoT = P/mgv, where P is the power consumption of all joints (motors). m and g are the mass of the robot (2.45 kg) and gravitational acceleration (9.81 m/s^2). v is the locomotion speed in m/s, obtained from $v = d/t$, where d is the distance traveled (here 1 m), and t is time in seconds for the traveled distance. The power consumption for the simulated robot cannot be determined directly by the simulation; therefore, it was calculated from $P = \tau \cdot \omega$, where τ and ω are motor torque (N·m) and motor angular speed (rad/s), respectively. The motor torque and angular speed are provided by the physical simulation CoppeliaSim. By contrast, the power consumption for the physical robot was calculated from $P = I \cdot V$, where I is electric current in amperes used by all motors during locomotion 1 m. It was measured using the integrated current sensors of the used Dynamixel XM430-W350 motors from ROBOTIS. V is voltage (here 12 V). For both simulated and real robots, we integrated the power consumption of all motors over time, summed it up, and calculated the average.

A. Body Pattern Analysis for Transition Strategy Synthesis

To synthesize a body-wave transition strategy suitable for climbing at each slope angle, we searched the space of body movements and used a reverse engineering approach to create the rules of the body-wave transition strategy to achieve the best climbing performance. To this end, we conducted a series of experiments that compared the locomotion abilities of the simulated robot with different body patterns, from standing to traveling waves, and with different stride frequencies. Neural

[2]Note that transient states based on the CoT and speed information occurred between the 1st (starting point) and 3rd strides. Subsequently, they were converted to a steady state without any significant changes.

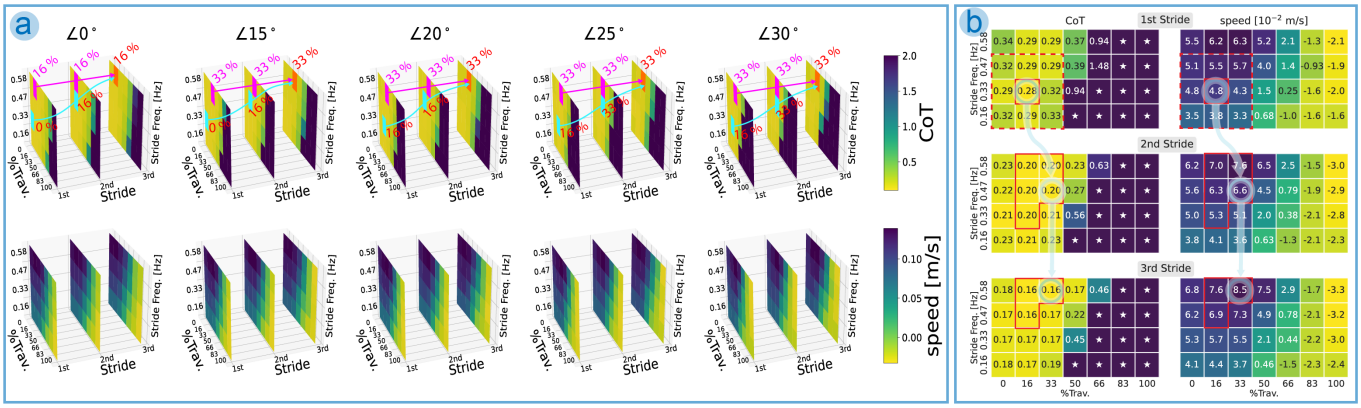

Fig. 3: (A) Locomotion performance (CoT and speed) under different body movements and slopes. CoT and speed are visualized in parallel for each slope angle. The blue arrow goes through the selected state (rectangle blue) to indicate body-wave transition strategies, whereas the pink arrow goes through the state of unchanging %Trav and stride frequency (rectangle pink) to indicate the constant body-wave movement. Eventually, both of them converted to the same steady state (rectangle orange). It can be seen that the body-wave transition strategy at a 15-degree angle shows the highest contrast, requiring three distinct values of %Trav, while other angles require only two different %Trav values. In the case of the constant body-wave strategy, only one %Trav value is utilized at each angle. (B) Detailed value of CoT and speed of the robot during the first three strides when the robot climbs on the maximum slope angle (30 degrees). The blue circle is the selected state, and the blue arrow indicates the transition of a state from the first to the third stride to illustrate the body-wave transition strategies. The red dashed boundary represents the neighboring states of a selected state (only shown at the 1st stride) and the dark red boundary represents the minimum CoT region for each stride. "⋆" indicates CoT > 2.0.

control drove the robot to perform a trot gait. Figure 3A presents the results of the search space of body movements. By analyzing a stride as the period for changing body patterns, we designed rules to decrease CoT and maximize velocity. To apply these rules, the gecko-inspired lateral undulation pattern that moves from slow to high speeds with standing and traveling waves, respectively, was considered one of the key aspects underlying robot locomotor capabilities. Therefore, we developed two rules for simultaneously changing body patterns during the first three strides and subsequently maintaining the patterns after the third stride.

(i) **1st stride:** select a state (state is described below) with a minimum average of CoT,

(ii) **2nd & 3rd strides:** change to a neighboring state in the minimum CoT region that exhibits the maximum velocity,

in this study, the state is represented as $\boldsymbol{S}^{slope}_{stride}$[%Trav (%Trav), stride frequency (Hz)] for better understanding. For example, $\boldsymbol{S}^{30^\circ}_{1st}$[16%Trav, 0.33Hz] indicates that the robot climbs at 30 degrees. During the 1st stride locomotion, the robot performs 16% of the traveling waves with a stride frequency of 0.33 Hz. Its neighboring states are indicated by a red dashed boundary in Fig. 3B. The dark red boundary indicates the minimum CoT region for each stride (see Fig. 3B).

Figure 3A presents an overview of the body-wave transition strategies for all slopes. Each slope (vertical column) was visualized parallel to the CoT and speed by capturing the first three strides. The CoT and speed for each stride are shown in detail at 30 degrees in Fig. 3B, in which the blue arrow passes through the selected state (Fig. 3A, blue rectangle) of the 1st, 2nd and 3rd stride to indicate how the robot continuously changes its body movements. The orange rectangle represents a steady state that is fixed after moving three strides. The pink arrow goes directly straight without any change in the stride frequency and %Trav (Fig. 3A, rectangle pink) though the same state as the steady state of each strategy. This was based on climbing performance measured across the space of body movements, which showed that the steady state (Fig. 3A, orange rectangle) is the state of "best performance" (i.e., low CoT and optimal speed) for the constant body-wave movement. In the following experiment, we compared the climbing performance of these constant body-wave movements (pink arrow) to the body-wave transition strategy (blue arrow) for each slope angle.

Specifically, Fig. 3B shows an example of a body-wave transition strategy, in which the robot climbs at the highest slope angle 30 degrees. The surface response results of CoT (left) and speed (right) are shown from top (1st stride) to bottom (3rd stride). We demonstrated a body-wave transition strategy from the first to third stride by following the rule step-by-step as described below:

(i) **1st stride:** we select the lowest average of CoT (0.28), such that the robot begins climbing at 30 degrees with a %Trav of 16% and a stride frequency of 0.33 Hz. At the moment, the speed of the robot is 0.048 m/s. The blue circle indicates the selected state $\boldsymbol{S}^{30^\circ}_{1st}$[16%Trav, 0.33Hz] (see Fig. 3B, 1st stride), and the blue arrow represent the state transition,

(ii) **2nd stride:** we move to the next state $\boldsymbol{S}^{30^\circ}_{2nd}$[33%Trav, 0.47Hz], which is a neighboring state located in the minimum CoT region, and exhibits highest speed in the region. In this state, we observed that CoT = 0.20 and speed = 0.066 m/s (see Fig. 3B, 2nd stride),

(iii) **3rd stride:** we proceed to the steady state $\boldsymbol{S}_{3rd}^{30^\circ}$[33%Trav, 0.58Hz], which is also a neighboring state in the minimum CoT region and has the highest speed. At its maximum speed of 0.085 m/s, the robot consumes 0.16 of CoT (see Fig. 3B, 3rd stride),

to sum up, a body-wave transition strategy for climbing at 30 degrees is a series of state: $\boldsymbol{S}_{1st}^{30^\circ}$[16%Trav, 0.33Hz], $\boldsymbol{S}_{2nd}^{30^\circ}$[33%Trav, 0.47Hz], and $\boldsymbol{S}_{3rd}^{30^\circ}$[33%Trav, 0.58Hz] from the first, second, and third strides, respectively.

In addition to developing a body-wave transition strategy, we obtained valuable knowledge regarding robot locomotion by searching a large space of body movements. Our findings can be summarized as follows. **i)** We found that the stride frequency of 0.16 Hz is extremely slow for our robot because it climbs at the lowest speed; however, the CoT does not reach the lowest values. Therefore, our strategy always starts with a higher stride frequency of 0.33 Hz on the first stride. **ii)** At the same slope, the robot trots slowly with a standing wave or fewer numbers of %Trav while moving faster with a larger number of %Trav to obtain a minimal CoT. For example, at a 15-degree slope, the robot bends its body by performing a standing wave at a slow speed of 0.33 Hz while performing 33% of traveling waves at a high speed of 0.58 Hz to reduce CoT. **iii)** At the first stride, the traveling waves tend to achieve higher climbing performance when the slope angle increases. Specifically, our strategy starts with standing waves when the robot climbs at 0 and 15 degrees. However, at slope angle greater than 15 degrees, the robot initially bends more traveling waves to 16 %Trav. This indicates that the body pattern influences not only the climbing speed but also the slope angle at which the robot climbs. Similarly, the effect of the slope angle on lateral bending was observed in Gekko geckos [18]. **iv)** The maximum acceptable value of %Trav for this simple leg trajectory is 33%. Consequently, we can define the robot's regular operating area (i.e., guarantee moving forward with acceptable energy consumption and speed), in which the stride frequency and %Trav range from 0.33-0.58 Hz and 0-33%, respectively, and the slope angle is less than 30 degrees.

B. Simulated Robot Climbing Experiments

To verify the locomotion performance of our body-wave transition strategies, five main experiments were conducted with different body movements when the 3-DoFs simulated robot climbed different slope angles (0, 15, 20, 25, and 30 degrees). This climbing experiment evaluated the energy efficiency during locomotion with body undulation using body-wave transition strategies compared with constant body-wave movement. Ten experimental results of each condition were recorded throughout the traversal of a one-meter distance. Furthermore, we compared the results of the 3-DoFs body configuration with a body configuration featuring fewer degrees of freedom and reduced weight–specifically, a 2-DoFs body configuration with a total robot weight of 2.27 kg, representing a 7.35% weight reduction. Note that we excluded a 1-DoF body configuration since it cannot generate a traveling wave (or constant wave).

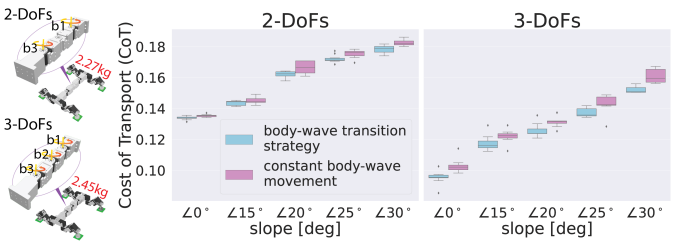

Fig. 4: Comparison of CoT between the body-wave transition strategy and constant body-wave movement of the simulated robots with 2-DoFs and 3-DoFs body joints at each slope angle. A video of this can be viewed at https://bit.ly/3PdOUpI.

The results (Fig. 4) show that the CoT of the simulated 2-DoFs and 3-DoFs robots with body-wave transition strategies were approximately 2.35-6% lower than that of the constant body-wave movement when the robots moved on the same slope angle. More specifically, for a slope angle of 30 degrees, the body-wave transition strategy robots with the 2-DoFs body and 3-DoFs body consumed approximately 0.1781±0.0025 and 0.1520±0.0018 of CoT, respectively, whereas the constant body-wave movement robots with the 2-DoFs body and 3-DoFs body consumed approximately 0.1825±0.0019 and 0.1609±0.0043, respectively. This indicates that initially moving from a slow speed with a body pattern of (close to) standing wave and then slightly increasing the speed and percentage of the traveling wave have a significant effect on climbing performance in term of energy efficiency. When comparing the 2-DoFs and 3-DoFs body configurations at each slope angle, the 3-DoFs body consistently demonstrates superior performance, outperforming the 2-DoFs body. This is because the 2-DoFs body is incapable of executing gecko-like smooth body undulation patterns [13], resulting in a climbing speed slower than that of the 3-DoFs body.

C. Physical Robot Climbing Experiments

To evaluate the locomotion performance of the body-wave transition strategy on physical robots, two robot versions were investigated for climbing at a slope angle of 30 degrees. The slope was constructed with an acrylic sheet on top of the plywood. For the first version, Slalom's original version is referred to as Mark-I (Fig. 5A), which was set up with EPDM rubber foot. The friction coefficient between EPDM rubber and acrylic is 0.58. For the second version, Slalom was modified and referred to as Mark-II (Fig. 5A) by implementing a pair of extension springs (a stiffness is 140 N/m for each spring) beside each body motor/joint as well as covering the robot feet with silicone rubber Dragon Skin 30, which has a friction coefficient of 0.87. These modifications involved increasing the difficulty in tracking the motor signal or the desired body-wave pattern, implying higher motor resistance or friction, and also increasing adhesion between the robot feet and surface.

Figure 5B depicts an example of dynamic tracking of the Mark-I robot with a body-wave transition strategy for climbing on a 30-degree slope, which is the skeleton of the body shown on the left, corresponding to the robot's posture shown on the right side. The continuous dots with

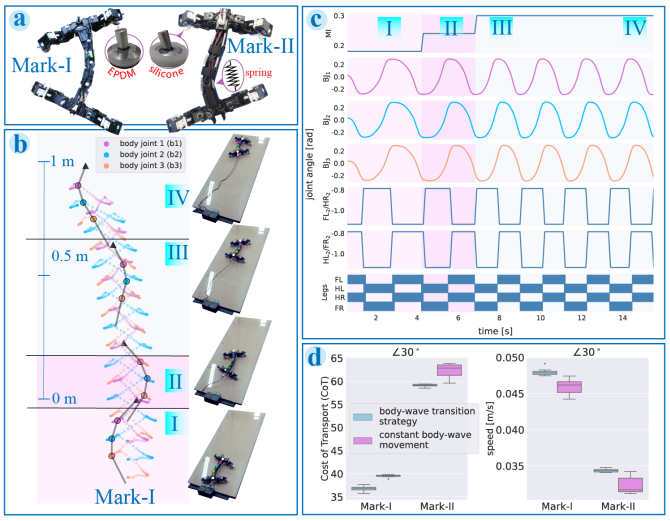

Fig. 5: Physical robot climbing experiment on a slope angle of 30 degrees. (A) Mark-I robot with EPDM rubber feet and Mark-II robot with extension springs beside each body segment and silicone rubber feet. (B) The dynamic tracking of the Mark-I robot with a body-wave transition strategy during traversing with its body skeleton and body joint trajectories. (C) Signals for body and leg joints and gait diagrams. (D) CoT and speed compared between the body-wave transition strategy and constant body-wave movement of both physical robots. A video of this can be viewed at https://bit.ly/3PdOUpI.

transparent colors of magenta, blue, and orange illustrate the joint trajectory of body joints 1, 2, and 3 respectively. The robot started with a slow speed and (closed to) a standing wave (i.e., state of $\boldsymbol{S}_{1st}^{30^\circ}$[16%Trav, 0.33Hz]), as the robot posture shown in Fig. 5B-I. The 2nd stride with an explicit state is $\boldsymbol{S}_{2nd}^{30^\circ}$[33%Trav, 0.47Hz], in which both %Trav and stride frequency were increased to 33 %Trav and 0.47 Hz, respectively (see Fig. 5B-II). Consequently, the robot stride to the third state of $\boldsymbol{S}_{3rd}^{30^\circ}$[33%Trav, 0.58Hz], in which this movement only increases the stride frequency to 0.58 Hz. Conversely, %Trav was still the same as the previous state. As the third stride was in the steady state, we allowed the robot to climb continuously with a constant steady state until it reached the goal distance of 1 meter. Figs. 5B-III and IV show examples of the body skeleton (left) and robot posture (right) during climbing after conversion to its steady state. Moreover, Fig. 5C depicts the temporal variation in the motor signals and a gait diagram in relation to Fig. 5B; their connections are indicated by blue Roman numeral labels.

As a result of 30-degree slope climbing, both physical robots (Mark-I and Mark-II) are consistent with those of the simulation robot, as they consistently demonstrate that the CoT consumption of the body-wave transition strategy is lower than that of a constant body-wave movement, even though their speeds are not significantly different. Specifically, Fig. 5D depicts a body-wave transition strategy of the Mark-I (Mark-II) robot consuming 36.8 (59.2) CoT at a velocity of 0.0479 (0.0345) m/s, whereas using a constant body-wave movement consumed an average of 39.6 (63.1) CoT at a velocity of 0.0462 (0.0320) m/s. The energy consumption for climbing was reduced by approximately 7% (6.5%) owing to the transition gradient of body movement. Additional analysis of the comparative performances of Mark-I and Mark-II can be accessed at https://bit.ly/3PdOUpI.

V. Discussion and Conclusion

We began by observing the gecko locomotion behaviors and found that they exhibit different patterns of lateral undulation during slow-speed trotting and high-speed running, with standing and traveling waves, respectively. From the analysis of gecko's body movement, we can demonstrate the 3-DoFs of its body joint trajectory and obtain a 4x phase difference between b1 and b2 that is greater than the phase difference between b2 and b3. Eventually, the phase ratio becomes ψ:0.25ψ, where ψ=$\frac{\pi}{3}$ radians. This gecko-inspired phase ratio was used to construct the phase relationship between each body joint and represent the waveform of the lateral undulation as a percentage of the traveling wave (%Trav). In Fig. 1C, the observed gecko body pattern can be represented as 50 %Trav.

We used a gecko-inspired robot, Slalom, consisting of 19 DoFs (three DoFs for the body and four DoFs per leg) to emulate gecko locomotion. The trotting gait of Slalom was controlled using CPG-based neural control with neuromodulation (MI). Elevating MI resulted in a corresponding increase in stride frequency. Using this robot as a scientific tool, we searched a large space of body movement parameters (i.e., %Trav and stride frequency) using the response surface method (RMS) to explore climbing performance at different slope angles. The climbing performance was evaluated based on CoT and locomotion speed. Exploring the gradient space of the body movement parameters during the first three strides enabled us to develop a body-wave transition strategy that proposes achieving energy-efficient climbing for each slope angle. Therefore, the experimental results of the simulated 2-DoFs and 3-DoFs robots with the body-wave transition strategy were approximately 2.35-6% lower than those of the constant body-wave strategy for all slopes. The physical robots consistently showed that the CoT of Mark-I (Mark-II) with a body-wave transition strategy was approximately 7% (6.5%) lower than that of the constant body-wave strategy at an angle of 30 degrees.

Moreover, we defined the operating area of the robot using body movement parameters, in which the stride frequency was between 0.33-0.58 Hz and %Trav was less than 33%. Compared with 50 %Trav, which has been observed in geckos, the robot was unable to cover the animal range of %Trav. This strengthens the idea that intercoordination between the body and legs is a key aspect in the locomotion skills of a sprawling pasture robot with a bendable body, such that the leg trajectory would be more complex for coordinating with a complex body pattern, such as a traveling wave. Typically, geckos exhibit complex leg trajectories during climbing [7].

Compared with existing studies (Table I), although standing and traveling waves have been observed in animals as part of their locomotor skills, the variety of body patterns and their transitions have not been sufficiently studied in robots,

particularly climbing robots. Most of them utilize standing waves to walk on the ground and traveling waves to swim in water or sand. For instance, salamander-like robots walk on the ground using standing waves and continuously transition to swimming in the water by switching to traveling waves with higher locomotion speeds [2] [3]. Recently, only a few robots have processed the benefits of having multiple body patterns for traversing hard surfaces, including a physical robot that was observed to use a traveling wave when controlled for turning [5] and a simulated robot that demonstrated a traveling wave when sensory-driven body-limb coordination was employed [17]. Consequently, our study is the first robot development to investigate the gradient of body patterns between standing and traveling waves and use body-wave transition strategies to efficiently transition from standing to traveling waves for climbing in both simulated and physical robots.

research, year	limb structure		multi segmented body (DoFs)	body-wave pattern		
	leg (DoFs)	adhesive foot*		standing	traveling	body-wave transition gradient
Our study	●●●●	✓	●●●	✓	✓	✓
Chong et al., 2022 [4]	●	✗	●●	✓	✓	✗
Suzuki et al., 2021 (Sim) [17]	●●	✗	●●●●	✓	✓	✗
Karakasiliotis et al., 2016 [3]	●●●●	✗	●●●●●	✓	✓	✗
Crespi et al., 2013 [2]	●	✗	●●●●	✓	✓	✗
Shura et al., 2021 [19]	●●	✗	●	✓	✗	✗
Schultz et al., 2021 [12]	●●	✓	●●	✓	✗	✗
Shao et al., 2022 [7]	●●●●	✓	✗	✗	✗	✗
Wang et al., 2023 [8]	●●●	✓	✗	✗	✗	✗
Nishad et al., 2022 [9]	●●	✓	✗	✗	✗	✗
Li et al., 2022 [10]	●●	✓	✗	✗	✗	✗

TABLE I: Comparison between our study and other state-of-the-art sprawling posture robot studies. "*" indicates a spacial foot structure design to enable the use of adhesive materials.

Furthermore, two reasons have been proposed in recent biological studies to explain why two lateral undulation patterns were exhibited. These patterns are intended to fulfill specific locomotor functions. The standing wave is associated with an increase in stride length, whereas the traveling wave contributes to the provision of more propulsion. Regarding energy transfer, the standing wave facilitates the conversion of kinetic and potential energy between the belly and the nodes throughout the stride cycle. However, energy propagation does not occur in a directional manner along the body. The phenomenon of energy propagation is observed through the mechanism of traveling waves. The axial muscles have the potential to function as both motors and struts, facilitating the transmission of propulsive forces generated by the limbs. In addition to these biological observations, we utilized robotics as a tool to help biologists formulate novel hypotheses regarding the energy efficiency of sprawling animals' locomotion. Based on the robot experiments, in which the robot's structure and body movements were directly inspired by the gecko's morphology and motion, respectively, the results indicated that performing a lateral undulation transition from standing to traveling provided energy efficiency for climbing. This suggests energy efficiency as a reason for geckos exhibiting two lateral undulations. In the future, we intend to enhance our CPG-based neural control framework by including premotor neural networks with a rapid learning algorithm to optimize the leg joint trajectories. The extension of the controller provides proper coordination between the leg and body undulations, allowing the robot to climb steeper slopes and be more energy efficient.

VI. Acknowledgments

We thank the CM labs for providing Vortex. This work was supported by the National Key R&D Program of China (2020YFB1313504)[PM, ZD].

References

[1] W. Wang, A. Ji, G. Chen, S. Ravi, H. Shen, S. N. Gorb, and Z. Dai, "Kinematics of gecko climbing: The lateral undulation pattern," *Zoology*, volume 140, page 125 768, 2020.

[2] A. Crespi, K. Karakasiliotis, A. Guignard, and A. J. Ijspeert, "Salamandra robotica ii: An amphibious robot to study salamander-like swimming and walking gaits," *IEEE Transactions on Robotics*, volume 29, number 2, pages 308–320, 2013.

[3] K. Karakasiliotis, R. Thandiackal, K. Melo, T. Horvat, N. K. Mahabadi, S. Tsitkov, J. M. Cabelguen, and A. J. Ijspeert, "From cineradiography to biorobots: An approach for designing robots to emulate and study animal locomotion," *Journal of The Royal Society Interface*, volume 13, number 119, page 20 151 089, 2016.

[4] B. Chong, T. Wang, E. Erickson, P. J. Bergmann, and D. I. Goldman, "Coordinating tiny limbs and long bodies: Geometric mechanics of lizard terrestrial swimming," *Proceedings of the National Academy of Sciences*, volume 119, number 27, e2118456119, 2022.

[5] T. Horvat, K. Melo, and A. J. Ijspeert, "Spine controller for a sprawling posture robot," *IEEE Robotics and Automation Letters*, volume 2, number 2, pages 1195–1202, 2017.

[6] S. Chevallier, A. Jan Ijspeert, D. Ryczko, F. Nagy, and J.-M. Cabelguen, "Organisation of the spinal central pattern generators for locomotion in the salamander: Biology and modelling," en, *Brain Res Rev*, volume 57, number 1, pages 147–161, Jul. 2007.

[7] D. Shao, Z. Wang, A. Ji, Z. Dai, and P. Manoonpong, "A gecko-inspired robot with cpg-based neural control for locomotion and body height adaptation," *Bioinspiration & Biomimetics*, volume 17, number 3, page 036 008, Apr. 2022.

[8] B. Wang, Z. Wang, Y. Song, W. Zong, L. Zhang, K. Ji, P. Manoonpong, and Z. Dai, "A neural coordination strategy for attachment and detachment of a climbing robot inspired by gecko locomotion," *Cyborg and Bionic Systems*, 2023.

[9] S. R. Nishad, R. Halder, G. Banda, and A. Thakur, "Development of a lizard-inspired wall-climbing robot using pressure sensitive adhesion," *IEEE Access*, volume 10, pages 72 535–72 544, 2022.

[10] X. Li, P. Bai, X. Li, L. Li, Y. Li, H. Lu, L. Ma, Y. Meng, and Y. Tian, "Robust scalable reversible strong adhesion by gecko-inspired composite design," *Friction*, volume 10, number 8, Aug. 2022.

[11] S. Bian, Y. Wei, F. Xu, and D. Kong, "A four-legged wall-climbing robot with spines and miniature setae array inspired by longicorn and gecko," *Journal of Bionic Engineering*, volume 18, number 2, pages 292–305, Mar. 2021.

[12] J. T. Schultz, H. K. Beck, T. Haagensen, T. Proost, and C. J. Clemente, "Using a biologically mimicking climbing robot to explore the performance landscape of climbing in lizards," *Proceedings of the Royal Society B: Biological Sciences*, volume 288, number 1947, page 20 202 576, 2021.

[13] W. Haomachai, D. Shao, W. Wang, A. Ji, Z. Dai, and P. Manoonpong, "Lateral undulation of the bendable body of a gecko-inspired robot for energy-efficient inclined surface climbing," *IEEE Robotics and Automation Letters*, volume 6, number 4, pages 7917–7924, 2021.

[14] W. Wang, A. Ji, Z. Dai, G. Qin, X. zhang, T. Ren, and Q. Han, "Angular variables of climbing geckos in two lateral undulation patterns," *Zoology*, volume 145, page 125 892, 2021.

[15] K. Karakasiliotis, N. Schilling, J.-M. Cabelguen, and A. J. Ijspeert, "Where are we in understanding salamander locomotion: Biological and robotic perspectives on kinematics," *Biological Cybernetics*, volume 107, number 5, pages 529–544, Oct. 2013.

[16] R. Ritter, "LATERAL BENDING DURING LIZARD LOCOMOTION," *Journal of Experimental Biology*, 1992.

[17] S. Suzuki, T. Kano, A. J. Ijspeert, and A. Ishiguro, "Spontaneous gait transitions of sprawling quadruped locomotion by sensory-driven body–limb coordination mechanisms," *Frontiers in Neurorobotics*, volume 15, 2021.

[18] Z. Wang, L. Cai, W. Li, A. Ji, W. Wang, and Z. Dai, "Effect of slope degree on the lateral bending in gekko geckos," *Journal of Bionic Engineering*, volume 12, number 2, pages 238–249, 2015.

[19] S. Shura, K. Takeshi, I. A. J., and I. Akio, "Sprawling quadruped robot driven by decentralized control with cross-coupled sensory feedback between legs and trunk," *Frontiers in Neurorobotics*, volume 14, 2021.